applied optics

Illumination-direction multiplexing Fourier ptychographic microscopy using hemispherical digital condensers

Maged Alotaibi,[1] Sueli Skinner-Ramos,[1,2,*] Ali Alamri,[1] Bader Alharbi,[1] Mohammed Alfarraj,[1] and Luis Grave de Peralta[1,2]

[1]Department of Physics, Texas Tech University, Lubbock, Texas 79409, USA
[2]Nano Tech Center, Texas Tech University, Lubbock, Texas 79409, USA
*Corresponding author: s.skinner-ramos@ttu.edu

Received 8 March 2017; revised 30 March 2017; accepted 10 April 2017; posted 11 April 2017 (Doc. ID 290217); published 5 May 2017

Simulations were conducted to explore a broader collection of possible illumination patterns realizable using a white-light-emitting hemispherical digital condenser. Several simple, but practical, illumination patterns were selected and used in experiments where a sample was illuminated simultaneously from different directions. The illumination-direction multiplexing (IDM) Fourier ptychographic microscopy (FPM) method was successfully used for imaging and phase recovery. This study suggests that IDM-FPM can be used for imaging photonic crystals with subwavelength periods using traditional microscope condensers with variable numerical aperture.

OCIS codes: (180.0180) Microscopy; (110.2990) Image formation theory; (110.2945) Illumination design; (230.3670) Light-emitting diodes.

https://doi.org/10.1364/AO.56.004052

1. INTRODUCTION

The simple substitution of the built-in illumination source of a common optical microscope by an array of light-emitting diodes (LEDs) [1–12] allows for the implementation of sophisticated microscope techniques [1–12]. In particular, Fourier ptychographic microscopy (FPM) [2,4,5,7–11] is based on the collection of several images obtained by illuminating the sample from different directions. FPM can provide image resolution below the Rayleigh resolution limit, $\sim\lambda/(2\mathrm{NA}_o)$, where λ is the vacuum wavelength of the light used for imaging, and NA_o is the numerical aperture of the microscope's objective lens [13–15]. Moreover, FPM is very useful since it can recover the unmeasured phase of the optical disturbance at the sample plane [2,12,15]. Originally, FPM was developed assuming incident illumination from a single direction at the time [2,12]. This required the collection of a large number of images and long exposure times, due to the low intensity of the LED [4,5]. Illuminating the sample simultaneously from multiple directions is a natural solution to this problem; therefore, a FPM phase-recovery algorithm capable of illumination-direction multiplexing (IDM) was readily demonstrated [4,5]. In this work, we explore the use of a hemispherical digital condenser (HDC) [6,7,10–12] to implement IDM-FPM. The distance of each LED in the HDC to the sample is equal to the HDC radius, which allows uniform illumination of the sample from every direction [6,7]. First, we conducted simulations in order to determine illumination patterns realizable using a HDC, which could be successfully used to implement IDM-FPM. We identify several simple, but practical, illumination patterns and experimentally demonstrated IDM-FPM with them. In particular, we found that the IDM-FPM technique with ring-like illumination patterns could be used for imaging photonic crystals. This is important because illuminating a sample with the ring of light produced by a condenser is one of the oldest but more effective ways to increase image resolution [16–18]. Therefore, our findings suggest that IDM-FPM can be used for imaging photonic crystals with subwavelength periods using traditional microscope condensers with variable numerical aperture. The rest of this paper is organized as follows: in Section 2 we present simulations of IDM-FPM. In Section 3 we describe the experimental setup used in this work, and compare the experimental and simulation results. Finally, the conclusions of this work are presented in Section 4.

2. IDM-FPM SIMULATIONS

As shown in block (1) in Fig. 1(a) the IDM-FPM algorithm starts (iteration index $m = 0$) by assuming an arbitrary amplitude ($a_{m=0}(r)$) and phase ($p_{m=0}(r)$) of the optical disturbance (OD) at the microscope's real plane (RP), ($a(r)\exp(ip(r))$) [2,15]. Then, as shown in block (2) of Fig. 1(a) the initial

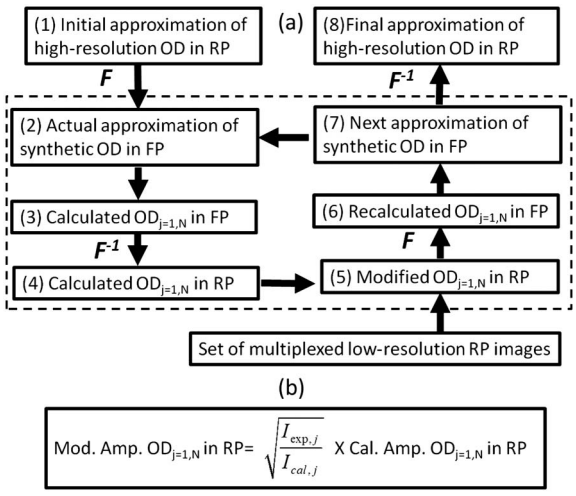

Fig. 1. (a) Flow chart of IDM-FPM phase-recovery algorithm steps. (b) The value of the modified amplitude of the OD in each RP point is proportional to the value of the calculated amplitude of the OD in the same RP point. The proportionality constant in each point depends on the ratio between the measured experimental intensity and the calculated intensity at that point.

approximation ($m = 1$, $j = 1$) for the actual OD at the microscope's Fourier plane (FP) is obtained by applying a two-dimensional (2D) Fourier transform (F) operation to the initial OD in the following way [2,15]:

$$A^{\text{act}}_{m=1,j=1}(k)e^{iP^{\text{act}}_{m=1,j=1}(k)} = F[a_{m=0}(r)e^{ip_{m=0}(r)}]. \quad (1)$$

Then, as sketched in block (3) in Fig. 1(a) the ODs associated to each of the single illumination directions (labeled $q = 1, 2, \ldots, N$), which contribute to the first ($j = 1$) multiplexed low-resolution RP image, are calculated as shown [2,12]:

$$A_{m,j,q}(k)e^{iP_{m,j,q}(k)} = A^{\text{act}}_{m,j}(k - k_q)e^{iP^{\text{act}}_{m,j}(k-k_q)} \cdot W_o, \quad q = 1, 2, \ldots, N, \quad (2)$$

where W_o is a circular window of radius NA_o and centered at $k = 0$. Equation (2) corresponds to the successive application of the operations "shift" and "window." First, the complex function describing the Fourier plane in the optical disturbance (FP-OD) is shifted toward the FP position k_q corresponding to the qth illumination direction. The shift is then followed by a multiplication by W_o, so that the resulting FP image is limited to an experimentally realizable numerical aperture (NA_o). As sketched in block (4) in Fig. 1(a), the ODs in the RP (RP-ODs) corresponding to each FP-OD are then obtained by applying an inverse 2D Fourier transform (F^{-1}) operation as follows [2,4,5]:

$$a_{m,j,q}(r)e^{ip_{m,j,q}(r)} = F^{-1}[A_{m,j,q}(k)e^{iP_{m,j,q}(k)}], \quad q = 1, 2, \ldots, N. \quad (3)$$

In single illumination-direction FPM, this step is followed by the substitution of the amplitude of the calculated RP-OD ($a_{m,j,q}(r)$) by the square root of the intensity of the corresponding experimental (or simulated) low-resolution RP image [2]. However, as sketched in block (5) in Figs. 1(a) and 1(b), in the IDM-FPM algorithm the amplitude of the calculated RP-ODs is modified in the following way [4,5]:

$$a^{\text{mod}}_{m,j,q}(r) = \sqrt{\frac{I_{\text{RP},j}}{I_{\text{RPT}}}}a_{m,j,q}(r), \quad I_{\text{RPT}} = \sum_{q=1}^{N} I_{\text{RP},j,q},\ I_{\text{RP},j,q} = [a_{m,j,q}(r)]^2, \quad (4)$$

where $I_{\text{RP},j}$ is the intensity of the experimental (or simulated) multiplexed low-resolution RP image number j. Equation (4) guarantees that the sum of all calculated intensities of the modified RP-ODs equals $I_{\text{RP},j}$. Moreover, Eq. (4) is equivalent to Eq. (5):

$$I_{\text{mod RP},j,q} = I_{\text{RP},j} - \frac{I_{\text{RP},j}}{I_{\text{RPT}}}\sum_{l\neq q} I_{\text{RP},j,l}, \quad I_{\text{mod RP},j,q} = [a^{\text{mod}}_{m,j,q}(r)]^2. \quad (5)$$

Equation (5) corresponds to the incoherent superposition condition requiring that the calculated intensity corresponding to a particular OD ($I_{\text{mod RP},j,q}$) should be equal to $I_{\text{RP},j}$ minus the sum of the intensities corresponding to all the others ODs contributing to the formation of the multiplexed low-resolution RP image number j. As sketched in block (6) in Fig. 1(a), the FP-ODs corresponding to each RP-OD are recalculated with the following equation [2,4,5]:

$$A^{\text{rec}}_{m,j,q}(k)e^{iP^{\text{rec}}_{m,j,q}(k)} = F[a^{\text{mod}}_{m,j,q}(r)e^{ip_{m,j,q}(r)}] \cdot W_o. \quad (6)$$

It is worth noting that the recalculated FP-ODs [block (6) in Fig. 1(a)] are improved versions of the previously calculated FP-ODs [block (3) in Fig. 1(a)] because the information contained in the experimental (or simulated) multiplexed images has been incorporated to the recalculated FP-ODs. Then, as sketched in block (7) of Fig. 1(a), the next approximation of the synthetic FP-OD is calculated in the following way [4,5]:

$$A^{\text{up}\,d}_{m,j}(k)e^{iP^{\text{up}\,d}_{m,j}(k)} = A^{\text{act}}_{m,j}(k)e^{iP^{\text{act}}_{m,j}(k)} + \alpha\sum_{q=1}^{N}[\gamma A^{\text{rec}}_{m,j,q}(k + k_q)e^{iP^{\text{rec}}_{m,j,q}(k+k_q)} - \beta A_{m,j,q}(k + k_q)e^{iP_{m,j,q}(k+k_q)}]. \quad (7)$$

As shown by the arrow between blocks (7) and (2) in Fig. 1(a), after the synthetic FP-OD is updated, it is used as the actual approximation for the next multiplexed images ($j = 2, 3\ldots, M$). The operations included in the box with the discontinuous line in Fig. 1 are successively done for each experimental (or simulated) multiplexed low-resolution RP image. This constitutes the first algorithm iteration ($m = 1$). The algorithm should converge after several iterations. Finally, as shown in block (8) in Fig. 1(a), the amplitude and phase corresponding to the final high-resolution RP image is obtained by applying an inverse 2D Fourier transform of the complex function corresponding to the updated FP-OD. We conducted IDM-FPM simulations using, as the initial approximation of the RP-OD, $p(r) = 0$ and $a(r)$ equal to the square root of the intensity corresponding to the first multiplexed low-resolution RP image used in the algorithm. We assumed a

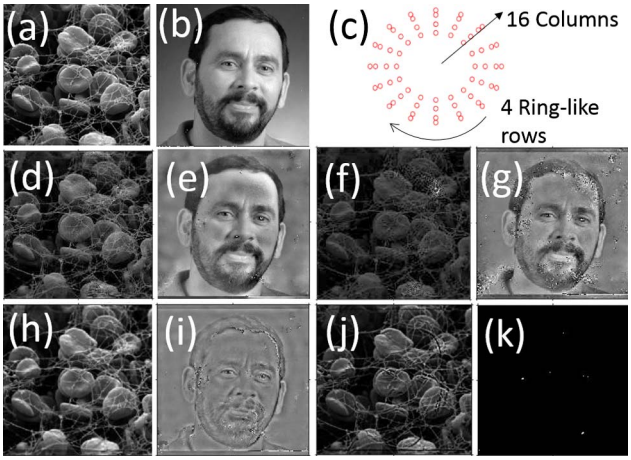

Fig. 2. IDM-FPM simulation results for arbitrary sample. (a), (b) Ideal OD, intensity, and phase, respectively. (c) Illumination direction distribution of LEDs in HDC. (d), (f), (h), (j) Intensity and (e), (g), (i), (k) phase corresponding to ODs obtained using the IDM-FPM algorithm with $NA_s = 1.77$. (d)–(k) Images obtained using IDM produced by simultaneously turning ON (d), (e) four and (j), (k) 16 consecutive LEDs in the same HDC row, (f), (g) four consecutive LEDs in the same HDC column, and (h), (i) 16 LEDs in each quarter of the HDC.

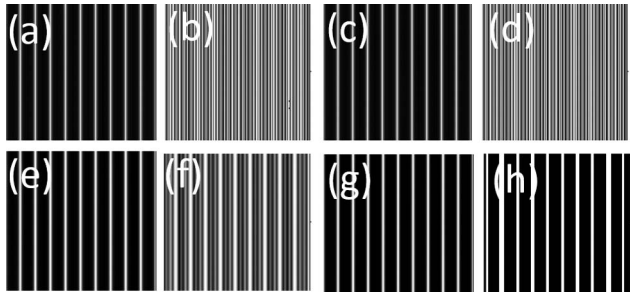

Fig. 3. IDM-FPM simulation results for a Ronchi ruling with a period of 1.67 μm. (a), (c), (e), (g) Intensities and (b), (d), (f), (h) phases corresponding to OD obtained using the IDM-FPM algorithm with $NA_s = 1.77$. Images (a), (b) and (g), (h) were produced using IDM with four and 16 consecutive LEDs in the same row, respectively, (c), (d) four consecutive LEDs in the same HDC column, and (e), (f) 16 LEDs in each quarter of the HDC. The same number of periods appear in all the images.

set of 64 illumination directions corresponding to each LED in a previously reported hemispherical digital condenser [6,7,10–12], which we also used in the experiments reported in this work. The HDC is formed by four ring-like rows with numerical aperture values of $NA_c = 0.58$, 0.73, 0.89, and 0.97. Rows contain 16 uniformly distributed LEDs each. Figure 2 shows simulation results corresponding to an arbitrary sample. This sample was selected to study the IDM-FPM capabilities on arbitrary non-periodic samples. Figures 2(a) and 2(b) show the ideal intensity and phase, respectively, which should be observed using perpendicular illumination and a synthetic numerical aperture $NA_s = NA_o + NA_c = 0.8 + 0.97 = 1.77$. A schematic of the LEDs illumination directions is shown in Fig. 2(c). Figures 2(d)–2(k) show the final intensities and phases corresponding to the RP-ODs obtained after 50 iterations of the IDM-FPM algorithm. The values $\alpha = 1$, $\beta = 0.5$, and $\gamma = 1$ were used in Eq. (7) for Figs. 2(d)–2(g), and the values $\alpha = 1$, $\beta = 0$, and $\gamma = 1$ for Figs. 2(h)–2(k).

Different combinations of α, β, γ values were explored (not shown) and the reported sets of values give the best results for an arbitrary sample. Figures 2(d)–2(g) and 2(h)–2(k) correspond to two successful and two partially successful illumination patterns, respectively. Partial success refers to poor or absent recovery of the phase. Nevertheless, the intensity of the final high-resolution multiplexed RP image was good in all cases. In each successful illumination pattern, four LED illumination directions were multiplexed and 16 low-resolution RP images were used. Figures 2(d) and 2(e) correspond to the set of illumination patterns formed by the 16 possible non-intercepting sets of four consecutive LEDs in the same HDC row simultaneously turned ON. Figures 2(f) and 2(g) correspond to the set of illumination patterns formed by the 16 possible non-intercepting sets of four consecutive LEDs in the same HDC column simultaneously turned ON. In each partially successful illumination pattern, 16 LED illumination directions were multiplexed and four low-resolution RP images were used. Figures 2(h) and 2(i) correspond to the set of illumination patterns formed by the four quarters of the HDC with 16 LEDs simultaneously turned ON in each quadrant. Figures 2(j) and 2(k) show the results obtained using the set of illumination patterns formed by the four HDC ring-like rows [Fig. 2(c)] with 16 LEDs simultaneously turned ON in each row. As shown in Fig. 3, the four illumination patterns discussed above produce more similar simulation results when used to illuminate samples with simpler structures. Figure 3 shows simulation results corresponding to a Ronchi ruling with a period $p = 1.67$ μm. Final intensities and phases corresponding to the RP-ODs, which were obtained after 50 iterations of the IDM-FPM algorithm and using the values $\alpha = 1$, $\beta = 0.5$, and $\gamma = 1$ in Eq. (7), are shown in Figs. 3(a)–3(d) and the values $\alpha = 1$, $\beta = 0$, and $\gamma = 1$ are shown in Figs. 3(e)–3(h). Figures 3(a), 3(c), 3(e), 3(g), and 3(b), 3(d), 3(f), 3(h) show the intensities and phases, respectively, corresponding to ODs obtained using the IDM-FPM algorithm with IDM produced by simultaneously turning ON four [Figs. 3(a) and 3(b)] and 16 [Figs. 3(g) and 3(h)] consecutive LEDs in the same HDC row, four consecutive LEDs in the same HDC column [Figs. 3(c) and 3(d)], and 16 LEDs in each quarter of the HDC [Figs. 3(e) and 3(f)]. Almost identical intensity images are obtained in all cases.

Details in the phase variate from one IDM pattern to another, but all of them show the same basic periodicity observed in the intensity images.

3. EXPERIMENTAL RESULTS

Details of the experimental setup used in this work, whose schematic illustration is shown in Fig. 4, can be found elsewhere [7,10–12]. In short, we used a Nikon Ti Eclipse inverted microscope equipped with a $NA_o = 0.8$ objective lens and a HDC as the illumination source. Two charged-coupled device cameras are attached to the microscope to obtain the RP and FP

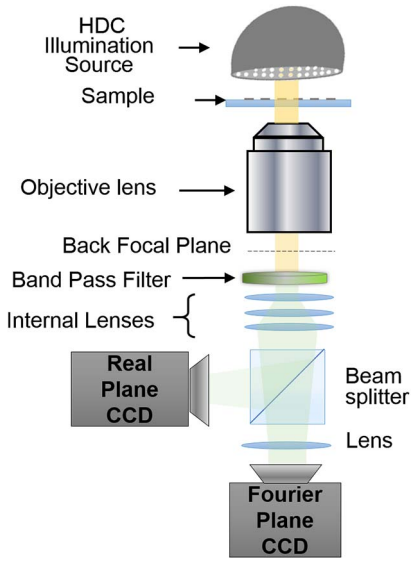

Fig. 4. Schematic of the experimental setup.

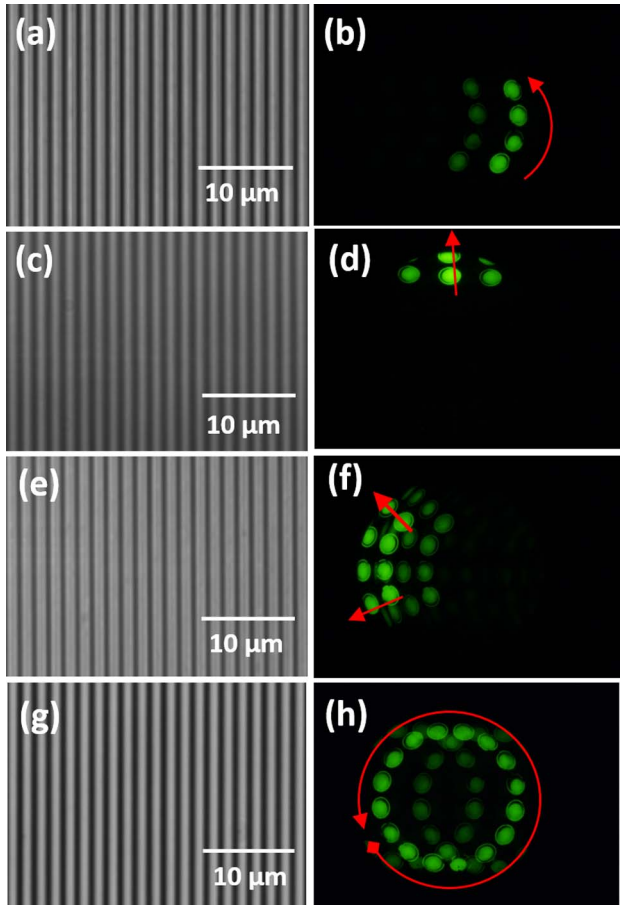

Fig. 5. Examples of experimental FP and RP images obtained with a $NA_o = 0.8$ objective lens, and by simultaneously turning ON (a), (b) four and (g), (h) 16 consecutive LEDs in the same HDC row, (c), (d) four consecutive LEDs in the same HDC column, and (e), (f) 16 LEDs in each quarter of the HDC. Arrows added to FP images group consecutive zero-order diffraction spots corresponding to the IDM pattern used.

images of the Ronchi ruling with $p = 1.67$ μm. A 10 nm bandpass filter centered at 570 nm wavelength was placed after the objective lens.

The HDC is formed by four concentric ring-like rows with numerical aperture values of $NA_c = 0.58$, 0.73, 0.89, and 0.97. Each LED that makes up the HDC can be turned ON/OFF independently. In our experiment, we selected different configurations of LEDs: four consecutive LEDs in the same row, four consecutive LEDs in the same column, 16 LEDs in a full quarter of the HDC, and 16 consecutives LEDs in the same row. Each configuration was iteratively cycled around the HDC until every LED was used. The HDC was placed, centered directly on top of the sample.

Figure 5 shows examples of experimental RP and FP multiplexed images corresponding to a Ronchi ruling with period $p = 1.67$ μm that were obtained using the experimental setup sketched in Fig. 4 and each of the four kinds of IDM patterns described in the previous section. It is worth noting that FP images are not used in the IDM-FPM algorithm; however, we used them for the exact determination of the illumination direction corresponding to each LED in the HDC. In addition, as shown in Figs. 5(b), 5(d), 5(f), and 5(h), we used the experimental FP images to illustrate the IDM pattern used in each case. The brightest spots in the FP images are zero-order diffraction spots corresponding to the illumination direction of a LED turned ON. Additional spots visible in the FP images are high-order diffraction spots. The arrows added to the FP images indicate the IDM patterns used. Figures 5(a) and 5(b) show an example of the 16 pairs of RP-FP images obtained using the IDM produced by four consecutives LEDs in the same HDC row, with $NA_c = 0.58$, simultaneously turned ON. Figures 5(c) and 5(d) show an example of the 16 pairs of RP-FP experimental images obtained using the IDM produced by four consecutive LEDs in the same HDC column simultaneously turned ON. Only two zero-order diffraction spots corresponding to LEDs in the HDC rows with $NA_c = 0.58$ and 0.73 are visible in the FP image shown in Fig. 5(d). The two missing zero-order diffraction spots were not collected by the microscope objective lens because they correspond to LEDs in the HDC rows with $NA_c > NA_o$. Figures 5(e) and 5(f) show an example of the four pairs of RP-FP experimental images obtained using the IDM produced by 16 LEDs occupying the same HDC quarter that are simultaneously turned ON. Similarly, only eight zero-order diffraction spots corresponding to LEDs in the HDC rows with $NA_c = 0.58$ and 0.73 are visible in the FP image shown in Fig. 5(f). The other eight zero-order diffraction spots were not collected by the microscope objective lens because they correspond to LEDs in the HDC rows with $NA_c > NA_o$. Figures 5(g) and 5(h) show an example corresponding to $NA_c = 0.58$ of the four pairs of RP-FP experimental images obtained using the IDM produced by 16 LEDs in the same HDC row simultaneously turned ON. As expected, in all experimental RP images the periodicity of the Ronchi ruling can be clearly seen because $p \gg \lambda/NA_o$ [13–16]. Nevertheless, these sets of experimental RP images are perfectly suited for a quantitative testing the phase-recovery capabilities of the IDM-FPM

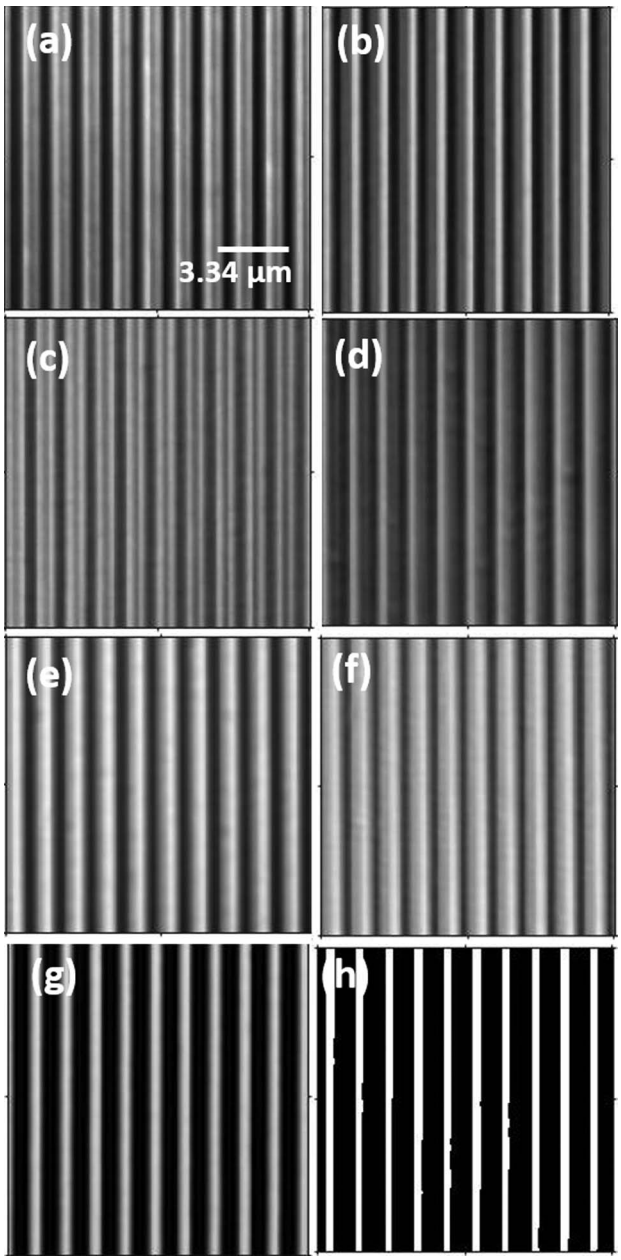

Fig. 6. IDM-FPM results using experimental multiplexed RP images. (a), (c), (e), (g) Intensities and (b), (d), (f), (h) phases corresponding to OD obtained using the IDM-FPM algorithm with the IDM produced by simultaneously turning ON (a), (b) four and (g), (h) 16 consecutive LEDs in the same HDC row, (c), (d) four consecutive LEDs in the same HDC column, and (e), (f) 16 LEDs in each quarter of the HDC. The same number of periods appear in all the images.

algorithm when the simple, but practical, illumination patterns discussed in the previous section are used.

Figures 6(a), 6(c), 6(e), 6(g), and 6(b), 6(d), 6(f), 6(h) show the intensities and phases, respectively, corresponding to ODs calculated using the IDM-FPM algorithm and multiplexed RP images. IDM was produced by simultaneously turning ON four [Figs. 6(a) and 6(b)] and 16 [Figs. 6(g) and 6(h)] consecutive LEDs in the same HDC row, four consecutive LEDs in the same HDC column [Figs. 6(c) and 6(d)], and 16 LEDs in each quarter of the HDC [Figs. 6(e) and 6(f)]. In excellent correspondence with the simulation results shown in Fig. 3, in all the images shown in Fig. 6 the correct periodicity of the Ronchi ruling is clearly observed. In particular, the results shown in Figs. 6(g) and 6(h) and Figs. 3(g) and 3(h) demonstrate that IDM-FPM using ring-like illumination permits to obtain the OD corresponding to a photonic crystal sample. It should be noted that the relatively large period of the Ronchi ruling used in our experiments does not allow one to appreciate the well-known improvement to the resolution of the numerically reconstructed RP image, which is characteristic of the FPM technique [2,9]. The resolution enhancement is easily seen by the obtained synthetic FP image with $NA_s > NA_o$ where diffraction spots corresponding to several diffraction orders are clearly observed (not shown). This distinguishes FPM from other techniques allowing phase recovery without resolution improvement [19,20].

4. CONCLUSIONS

We explored the implementation of IDM-FPM using a HDC. Good correspondence between experiment and simulations demonstrated that this can be accomplished using several simple, but practical, illumination patterns. In particular, when using ring-like illumination patterns IDM-FPM permits to find the OD corresponding to relatively simple samples like photonic crystals. This suggests the exciting possibility to combine IDM-FPM and the use of traditional microscope condensers with variable NA_c for imaging photonic crystals with subwavelength resolution.

REFERENCES

1. G. Zheng, C. Kolner, and C. Yang, "Microscopy refocusing and dark-field imaging by using a simple LED array," Opt. Lett. **36**, 3987–3989 (2011).
2. G. Zheng, R. Horstmeyer, and C. Yang, "Wide-field, high-resolution Fourier ptychographic microscopy," Nat. Photonics **7**, 739–745 (2013).
3. Z. Liu, L. Tian, S. Liu, and L. Waller, "Real-time brightfield, darkfield, and phase contrast imaging in a light-emitting diode array microscope," J. Biomed. Opt. **19**, 106002 (2014).
4. S. Dong, R. Shiradkar, P. Nanda, and G. Zheng, "Spectral multiplexing and coherent-state decomposition in Fourier ptychographic imaging," Biomed. Opt. Express **5**, 1757–1767 (2014).
5. L. Tian, X. Li, K. Ramchandran, and L. Waller, "Multiplexed coded illumination for Fourier ptychography with LED array microscope," Biomed. Opt. Express **5**, 2376–2389 (2014).
6. D. Dominguez, L. Molina, D. B. Desai, T. O'Loughlin, A. A. Bernussi, and L. Grave de Peralta, "Hemispherical digital optical condensers with no lenses, mirrors, or moving parts," Opt. Express **22**, 6948–6957 (2014).
7. S. Sen, L. Molina, D. Cao, D. B. Desai, A. A. Bernussi, and L. Grave de Peralta, "Versatile optical microscopy using a reconfigurable hemispherical digital condenser," Biomed. Opt. Express **6**, 658–667 (2015).
8. K. Guo, S. Dong, P. Nanda, and G. Zheng, "Optimization of sampling pattern and the design of Fourier ptychographic illuminator," Opt. Express **23**, 6171–6180 (2015).
9. X. Ou, R. Horstmeyer, G. Zheng, and C. Yang, "High numerical aperture Fourier ptychography: principle, implementation and characterization," Opt. Express **23**, 3472–3491 (2015).
10. S. Sen, D. B. Desai, M. H. Alsubaie, M. V. Zhelyeznyakov, L. Molina, H. Sari-Sarraf, A. A. Bernussi, and L. Grave de Peralta, "Imaging photonic crystals using Fourier plane imaging and Fourier ptychographic

microscopy techniques implemented with a computer-controlled hemispherical digital condenser," Opt. Commun. **383**, 500–507 (2016).
11. S. Sen, A. Ishtiaque, B. Aljubran, A. A. Bernussi, and L. Grave de Peralta, "Fourier ptychographic microscopy using an infrared-emitting hemispherical digital condenser," Appl. Opt. **55**, 6421–6427 (2016).
12. D. B. Desai, S. Sen, M. V. Zhelyeznyakov, W. Alenazy, and L. Grave de Peralta, "Super-resolution imaging of photonics crystals using the dual-space microscopy technique," Appl. Opt. **55**, 3929–3934 (2016).
13. J. W. Goodman, *Introduction to Fourier Optics* (McGraw-Hill, 1968).
14. E. Hecht, *Optics*, 3rd ed. (Addison-Wesley, 1998).
15. M. Born and E. Wolf, *Principles of Optics*, 5th ed. (Pergamon, 1975).
16. H. H. Hopkins and P. M. Barham, "The influence of the condenser on microscopic resolution," Proc. Phys. Soc. **63**, 737–744 (1950).
17. D. B. Desai, D. Dominguez, A. A. Bernussi, and L. Grave de Peralta, "Ultra-thin condensers for optical subwavelength resolution microscopy," J. Appl. Phys. **115**, 093103 (2014).
18. D. B. Desai and L. Grave de Peralta, "Optical condensers formed in wet-mounting setup," Appl. Opt. **54**, 3580–3587 (2015).
19. S. Mehta and C. Sheppard, "Quantitative phase-gradient imaging at high resolution with asymmetric illumination-based differential phase contrast," Opt. Lett. **34**, 1924–1926 (2009).
20. K. Guo, Z. Bian, S. Dong, P. Nanda, Y. Wang, and G. Zheng, "Microscopy illumination engineering using low-cost liquid crystal display," Biomed. Opt. Express **6**, 574–579 (2015).